A High-Capacity Polyethylene Oxide-Based All-Solid-State Battery Using Metal-Organic Framework Hosted Silicon Anode

Leicheng Zhang[a,1], Yanke Lin[a,1], Xudong Peng[a], Maochun Wu[c,*], Tianshou Zhao[a,b,*]

[a] Department of Mechanical and Aerospace Engineering, The Hong Kong University of Science and Technology, Clear Water Bay, Kowloon, Hong Kong SAR, China

[b] Department of Mechanical and Energy Engineering, Southern University of Science and Technology, Shenzhen, 518055, China

[c] Department of Mechanical Engineering, The Hong Kong Polytechnic University, Hung Hom, Kowloon, Hong Kong SAR, China

[1] These authors contributed equally to this work.

* Corresponding authors:

E-mail: maochun.wu@polyu.edu.hk (M.C. Wu)

E-mail: metzhao@ust.hk, zhaots@sustech.edu.cn (T.S. Zhao)

Abstract

Polyethylene oxide (PEO)-based solid electrolytes have been widely studied in all-solid-state lithium (Li) metal batteries due to their favorable interfacial contact with electrodes, facile fabrication, and low cost, but their inferior Li dendrite suppression capability renders low actual areal capacities of Li metal anodes. Here, we develop a high-capacity all-solid-state battery using a metal-organic framework hosted silicon (Si@MOF) anode and a fiber-supported PEO/garnet composite electrolyte. Si nanoparticles are embedded in the micro-sized MOF-derived carbon host, which efficiently accommodates the repeated deformation of Si over cycles while providing sufficient charge transfer pathways. As a result, the Si@MOF anode shows excellent interfacial stability toward the composite polymer electrolyte for over 1000 h and achieves a high reversible areal capacity of 3 mAh cm^{-2}. The full cell using the $LiFePO_4$ (LFP) cathode is able to deliver 135 mAh g^{-1} initially and maintains 73.1% of the capacity after 500 cycles at 0.5 C and 60 ℃. More remarkably, the full cells with high LFP loadings achieve areal capacities of more than 2 mAh cm^{-2}, exceeding most PEO-based ASSBs using metallic Li. Finally, the pouch cell using the proposed design exhibits decent electrochemical performance and high safety.

Keywords:

All-solid-state battery; silicon anode; PEO; composite polymer electrolyte; SEI

1. Introduction

The overwhelming trend of vehicle electrification worldwide has posed tremendous demands for power batteries with high energy density, long cycle life, and absolute safety.[1,2] Although lithium-ion batteries (LIBs) using graphite anodes have been widely used, they have gradually approached their limits on energy, and the flammable organic liquid electrolytes used in the LIBs also bring serious safety concerns.[3–5] To tackle the issues, all-solid-state batteries (ASSBs) using solid electrolytes (SEs) are regarded as promising future energy storage devices because they enable the possible use of Li metal anode with greatly improved security[6,7].

Unfortunately, persistent dendrite formation on metallic Li over cycles remains unresolved yet, which will lead to the gradual electrode degradation and final short-circuiting, hampering the large-scale implementation of ASSBs.[8] Moreover, due to the diffusion limitation in the Li metal electrode, ASSBs usually need to be operated at current densities lower than 1.0 mA cm^{-2} to avoid rapid dendrite-induced failure, which fails to meet the requirements for practical applications.[9,10] Hence, It is imperative to develop alternative anode materials for next-generation high-energy ASSBs.

Silicon (Si) is one of the most promising materials due to its high theoretical capacity (3600 mAh g^{-1}), similar lithiation potential (0.4 V vs. Li/Li^+) with that of graphite, and abundant reserves on earth.[11–13] Nonetheless, the large volume expansion and contraction of Si over cycles expose the fresh Si surface to the liquid electrolytes in traditional LIBs, which results in the continuous formation of solid-

electrolyte interphase (SEI) on the Si surface and poor cycling stability.[14,15] This issue can be greatly mitigated by replacing liquid electrolytes with rigid SEs, as the latter allow the use of high external pressure to constrain the deformation of Si anodes. Since the SEs are not replenished to the Si surface like liquid electrolytes, the contact area can be reduced to a two-dimensional (2-D) plane.[16–20] Si film electrodes were first proposed to pair with oxide or sulfide SEs, which could deliver high capacities over 2000 mAh g^{-1}. However, the cycling stability drastically deteriorated when the film thickness exceeded 1 μm, which rendered a low areal capacity of 0.5 mAh cm^{-2}, far below that of commercial graphite anodes (2-4 mAh cm^{-2}).[17,18,20] To increase the practical capacity, architecture design strategies have been implemented to relieve the huge stress generated during the cycling of bulk Si film electrodes. For instance, An amorphous Si film electrode was fabricated with a porous structure, which could effectively buffer the volume change and maintain the structural integrity.[21] A columnar Si electrode was combined with an argyrodite-type Li_6PS_5Cl with an external pressure of 25 MPa, which compensated the vertical expansion of columnar Si and thus enabled the formation of a stable 2-D lateral SEI. As a result, a high areal capacity of 3.5 mAh cm^{-2} was achieved for the Si anode and 2.7 mAh cm^{-2} for the full cell[22]. However, the above structures require sophisticated fabrication processes such as magnetron sputtering that may not be scalable. Recently, a low-cost micro-Si anode with a high Si content of 99.9 wt% showed remarkable performance enabled by the elimination of carbon and passivating ability of sulfide SE. It was demonstrated that a full cell with a high NCM811 cathode loading of 25 mg cm^{-2} achieved high capacity

retention of 80% after 500 cycles.[23]

Of reported works, although the oxide or sulfide SEs with high mechanical strength can restrain the SEI growth to a 2-D plane, high external pressures ranging from 20-370 MPa are necessary to resist the morphological changes and maintain the interfacial contact between the SEs and the Si electrodes, which may bring challenges for practical operation.[21–23] Compared to inorganic SEs, composite polymer electrolytes (CPEs) comprised of ceramics and polymers are flexible and thus can be operated without high external pressures.[24–26] Polyethylene oxide (PEO) is the most commonly used polymer matrix for CPEs due to its superb compatibility with Li salts, low interfacial resistance with anodes, facile preparation, and low cost.[27–29] Nevertheless, the inferior mechanical strength of PEO-based CPEs endows themselves with weaker dendrite suppression capability than the inorganic SEs, resulting in low critical current densities and limited actual areal capacities when paired with Li metal anodes[30–33]. However, since the dendrite issue is drastically diminished in the alloying-type Si anodes, they stand out as promising mates for PEO-based CPEs to break through the areal capacity limitation, on which rare work has been reported so far.

In this work, we develop a high-capacity ASSB using a metal-organic framework-derived carbon hosted Si (Si@MOF) anode with a polyvinylidene difluoride (PVDF) fiber supported PEO/garnet composite electrolyte (PPG). As illustrated in Figure 1a, the Si nanoparticles are embedded in the micro-sized MOF-derived carbon hosts that can provide sufficient conductive pathways and effectively buffer the repeated

volume variation. Additionally, the PVDF scaffold strengthens the composite electrolyte while the garnet fillers enhance the ionic conductivity. Benefiting from the integrated design, conformal interfacial contact between the Si@MOF anode and PPG can be achieved after softening of PPG at 60 ℃ and preserved over cycles, and therefore no high external pressure is required throughout battery operation. As a result, the Si@MOF anode shows excellent interfacial stability against PPG over cycles for 1200 h and achieves a high areal capacity of 3 mAh cm^{-2}. Furthermore, the full battery using $LiFePO_4$ (LFP) cathode is able to deliver a high initial capacity of 150 mAh g^{-1} at 0.2 C and retain 73.1% of its original capacity after 500 cycles at 0.5 C. More impressively, full cells with high LFP loadings and a pouch cell are assembled and show decent electrochemical performance. This work opens up a new avenue for the development of long-cycling and high-capacity ASSBs.

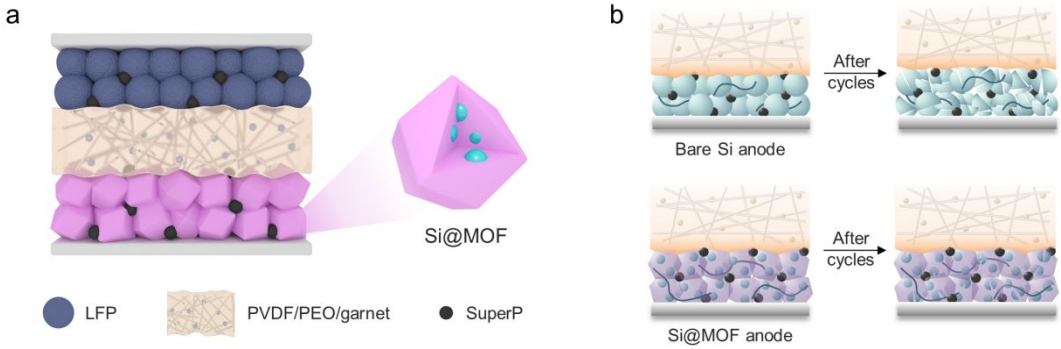

Figure 1. Schematic illustration of (a) the ASSB comprised of LFP | PVDF/PEO/garnet (PPG) | Si@MOF and (b) interfacial evolution between PPG and bare Si or Si@MOF anode.

2. Results and Discussion

2.1. Material characterizations of Si@MOF and PPG solid electrolyte

The Si@MOF structure was prepared by a facile hydrothermal method followed by calcination.[34] The morphology of the as-synthesized Si@MOF was revealed by scanning electron microscope (SEM) and transmission electron microscope (TEM) techniques. As shown in Figure 2a, the ZIF-67 derived carbon host exhibits a conformal polyhedral structure, and the sizes of the microparticles range from 600 nm to 1.1 μm (Figure S1). From the TEM image in Figure 2b, it can be clearly seen that the Si nanoparticles are successfully encapsulated in the ZIF-67 framework, which is also confirmed by the energy-dispersive X-ray spectroscopy (EDS) element mapping results (Figure 2c). The Si content is determined to be 64.4% by thermogravimetric analysis (TGA, Figure S2). Additionally, the cobalt (Co) metal center is conducive to improving the graphitization degree of the carbon coating during heat treatment, while the porous structure inherited from the ZIF-67 precursor can provide sufficient ionic conductive pathways.[35]

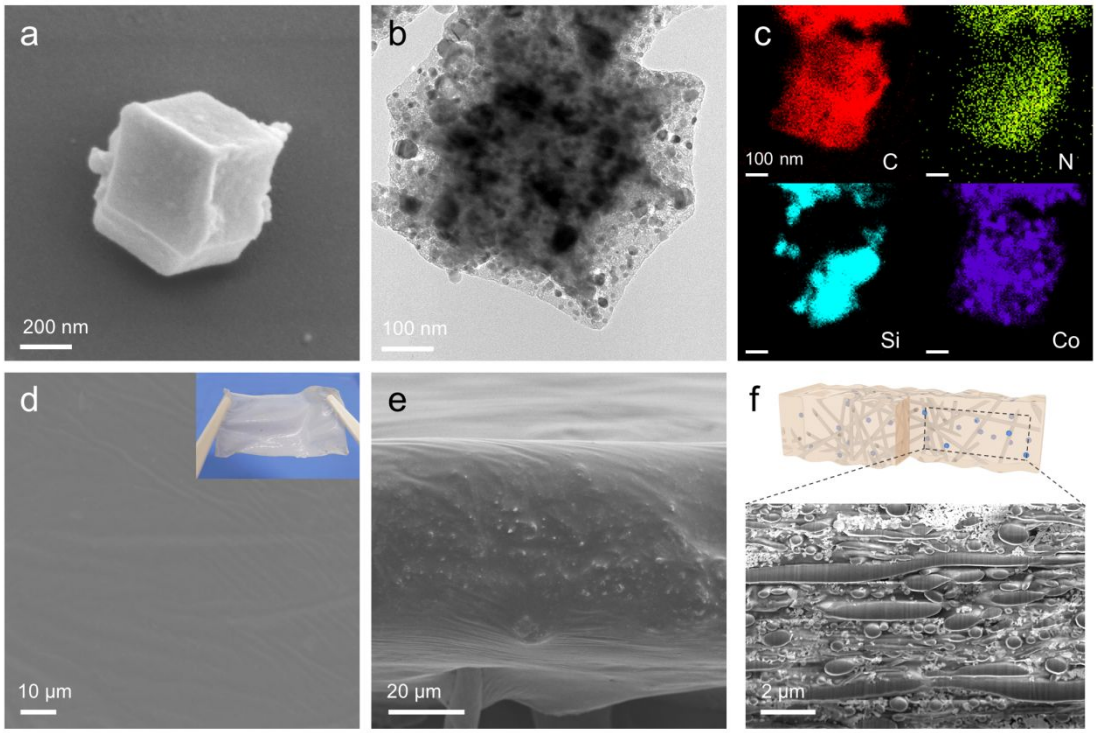

Figure 2. (a) SEM and (b) TEM image of Si@MOF structure and corresponding (c) EDS element mapping results of C, N, Si, and Co. SEM images of PPG from the (d) top and (e) cross-sectional views. Inset in (d) is the digital photo of PPG. (f) The inner structure of PPG after FIB cutting.

The PPG was fabricated by incorporating PEO and garnet-type $Li_{6.5}La_3Zr_{1.5}Ta_{0.5}O_{12}$ (LLZTO) into the PVDF fiber skeleton developed in our previous work.[7] Figure 2d shows the SEM image of the PPG from the top view, which indicates that the CPE has a rather smooth surface. As shown by the digital photo, the PPG exhibits good flexibility with a homogeneous appearance, suggesting that the garnet fillers are well dispersed. From the cross-sectional view, the thickness of the PPG is measured to be around 60 μm (Figure 2e). To further unveil the internal structure of the PPG, the focused ion beam (FIB) was used to cut it vertically and the exposed cross-section is displayed in Figure 2f. The round areas are attributed to the

PVDF fibers, and the small nanoparticles are the garnet grains that are uniformly distributed throughout the depth, which can contribute to the fast ion conduction through the electrolyte.[36] Figure S3 shows the X-ray diffraction (XRD) pattern of PPG and the peaks correspond well to the garnet-type $Li_5La_3Nb_2O_{12}$, suggesting that the crystal structure of LLZTO preserves well after the fabrication processes. The ionic conductivity of the PPG is measured to be 0.081 mS cm^{-1} at 25 ℃ (Figure S4), which is comparable with related works on PEO-based CPEs.[32,36]

2.2. Electrochemical characterizations of Si@MOF electrode with PPG

The electrochemical behavior of the Si@MOF electrode paired with PPG was first characterized in coin cells using Li metal as the counter electrode at 60 ℃. Bare Si electrodes with no modification were also prepared for comparison. Figure 3a shows the cycling performance at a current density of 200 mA g^{-1} based on the weight of Si. An initial lithiation capacity of 1967 mAh g^{-1} is delivered for the Si@MOF electrode and 1416 mAh g^{-1} is extracted during delithiation, giving a good initial coulombic efficiency (ICE) of 72.0%. On the contrary, the ICE of the bare Si electrode is only 50.8%, which indicates severe side reactions between the unprotected Si surface and the PPG. After 50 cycles, a high reversible capacity of 1442 mAh g^{-1} can be retained for the Si@MOF electrode, showing much enhanced cycling stability compared to the bare Si electrode (636 mAh g^{-1} after 50 cycles). From the voltage profiles in Figure 3b, the lithiation and delithiation potentials of the Si@MOF electrode remain almost unchanged over cycles while continuously increasing overpotential is observed in the

bare Si electrode upon cycling (Figure 3c). Cross-sectional SEM images were taken on the bare Si and Si@MOF electrodes before and after cycling (Figure S5). It can be observed that the bare Si electrode goes through a large volume expansion after cycling, and cracks and voids are found both inside the electrode and on the electrode/PPG interface. While for the Si@MOF electrode, the volume expansion is mitigated, and the interface is well preserved without signs of detachment, which can be attributed to the MOF-derived host that effectively accommodates the volume change of Si. Electrochemical impedance spectra (EIS) tests were performed on both electrodes after activation. Nyquist plots in Figure 3d show that the Si@MOF exhibits a lower charge transfer resistance than the bare Si electrode, suggesting more facile charge transfer through the SEI that is stabilized by the MOF-derived carbon host.

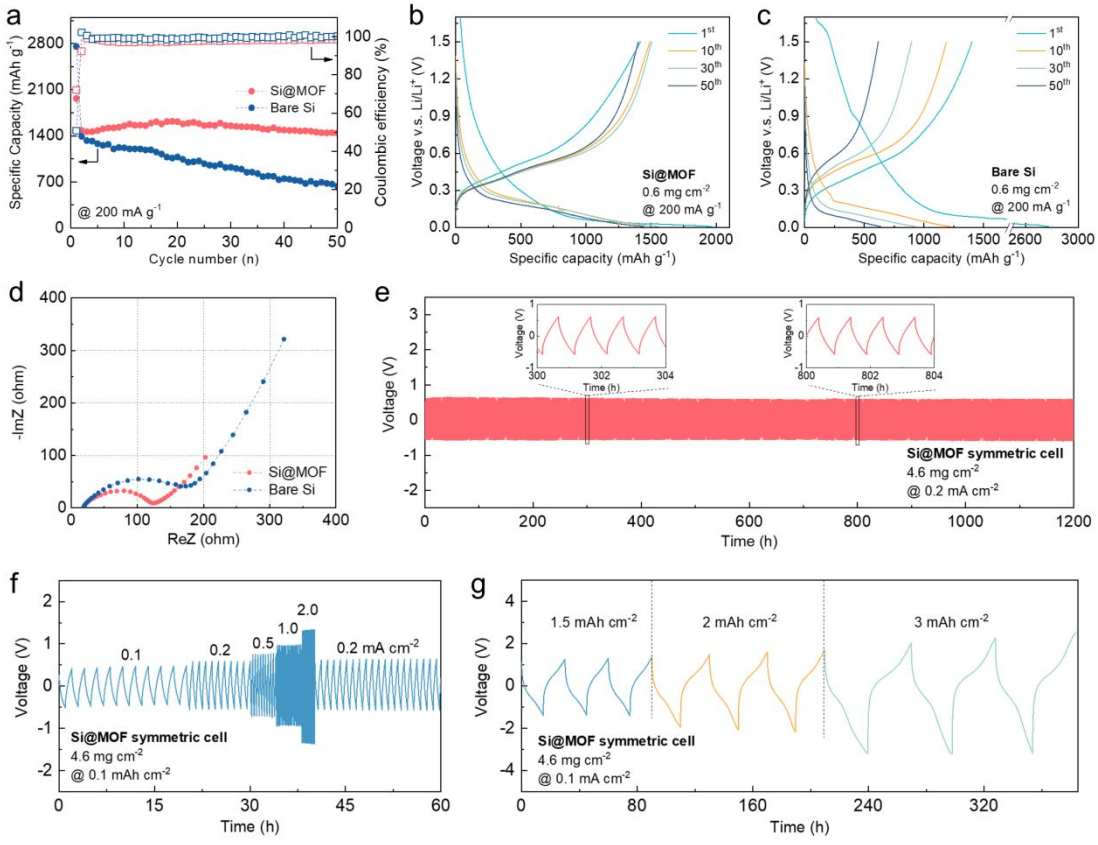

Figure 3. (a) Lithiation capacities of Si@MOF and bare Si electrode at 200 mA g^{-1}.

Representative voltage profiles of (b) Si@MOF and (c) bare Si electrodes. (d) Nyquist plots of two electrodes after activation cycles. Voltage profiles of Si@MOF symmetric cell cycling at (e) 0.2 mA cm^{-2} for 1200 h, (f) varying current densities, and (g) 1.5, 2, and 3 mAh cm^{-2} for 3 cycles each at 0.1 mA cm^{-2}. The cells were tested at 60 ℃.

Although the incorporation of PVDF skeleton and garnet particles can drastically enhance the mechanical strength of PPG, it is yet not able to completely suppress the Li dendrite formation. Actually, when the Li plating/stripping capacity of a Li | PPG | Li symmetric cell reaches 1.5 mAh cm^{-2}, the cell fails rapidly due to dendrite-induced short-circuit (Figure S6), which makes the Li metal an unsuitable counter electrode to characterize the Si anode in this study. Instead, symmetric cells using Si@MOF electrodes were assembled. Figure 3e exhibits the voltage profiles of repeated lithiation and delithiation at 0.2 mA cm^{-2} for 0.5 h each. The symmetric cell can be stably cycled for 1200 h with almost no change in overpotential, suggesting the excellent interfacial stability between Si@MOF anode and PPG. In sharp contrast, the symmetric cell using bare Si electrodes undergoes a rapid increase in overpotential after only 100 h (Figure S7), which can be explained by the SEI failure and loss of contact caused by the Si pulverization (Figure 1b). More remarkably, even at a high current density of 2 mA cm^{-2}, the Si@MOF symmetric cell can still exhibit a stable lithiation/delithiation process (Figure 3f). To further probe the capability to achieve high areal capacity, the Si@MOF symmetric cell was cycled at increasing capacities of 1.5, 2, and 3 mAh cm^{-2} for 3 cycles each. Figure 3g shows that the

lithiation/delithiation voltage profiles are steady with no signs of degradation or short-circuiting, which outperforms most reported values achieved in the Li metal anodes using PEO-based CPEs.[30–33]

2.3. Electrochemical performances of Si@MOF | PPG | LFP full cells

To further demonstrate the application possibility, ASSBs equipped with the proposed Si@MOF and PPG/LFP integrated cathodes were assembled in coin cells and tested at 60 ℃. The pre-lithiation capacity of Si anode was first controlled to be 100% of LFP cathode (N/P capacity ratio = 2) to compensate for the Li losses caused by SEI formation or Li trap during cycling. Figure 4a shows the discharge capacities of the full cells using two kinds of anodes at the current density of 0.2 C (1 C = 170 mAh g^{-1}_{LFP}). For the cell using bare Si anode, a capacity of 121 mAh g^{-1} is delivered for the first cycle but quickly decays to 86 mAh g^{-1} after 100 cycles. In sharp contrast, the Si@MOF anode enables the full cell to achieve a high reversible capacity of 148 mAh g^{-1} and maintain 136 mAh g^{-1} after 100 cycles, rendering a high retention rate of 91.9%. The average discharge potential of the Si@MOF cell is ~ 2.8 V as shown in Figure 4b, which is lower than that of the Li-LFP half cell due to the anode delithiation potential of ~ 0.4 V (vs. Li/Li^+).[7] The voltage profiles are quite steady within the first 100 cycles, suggesting good reversibility of the proposed full cell. Figure 4c and d display the discharge capacities and voltage profiles of the Si@MOF full cell at current densities of 0.1, 0.2, 0.5, and 1.0 C. At a high rate of 1.0 C, the Si@MOF full cell can still deliver a capacity of 108 mAh g^{-1}, indicating satisfactory

rate capability. A long-term cycling test was then performed on the Si@MOF full cell at 0.5 C. An excellent capacity retention rate of 73.1% is achieved after 500 cycles (Figure 4e), which demonstrates the remarkable cycling stability enabled by the Si@MOF anode and integrated cell design strategy. Furthermore, full cells with high LFP loadings were assembled and the N/P capacity ratio was reduced to 1.5 to imitate practical conditions. As shown in Figure 4f and g, areal capacities of 2.2 and 2.6 mAh cm^{-2} can be accomplished with the LFP loading of 15.4 and 20.2 mg cm^{-2} at 0.1 mA cm^{-2}, and the cells can be stably cycled at 0.2 mA cm^{-2} with areal capacities of 1-2 mAh cm^{-2} (Figure 4h). These results signify substantial progress in the development of ASSBs using PEO-based electrolytes.

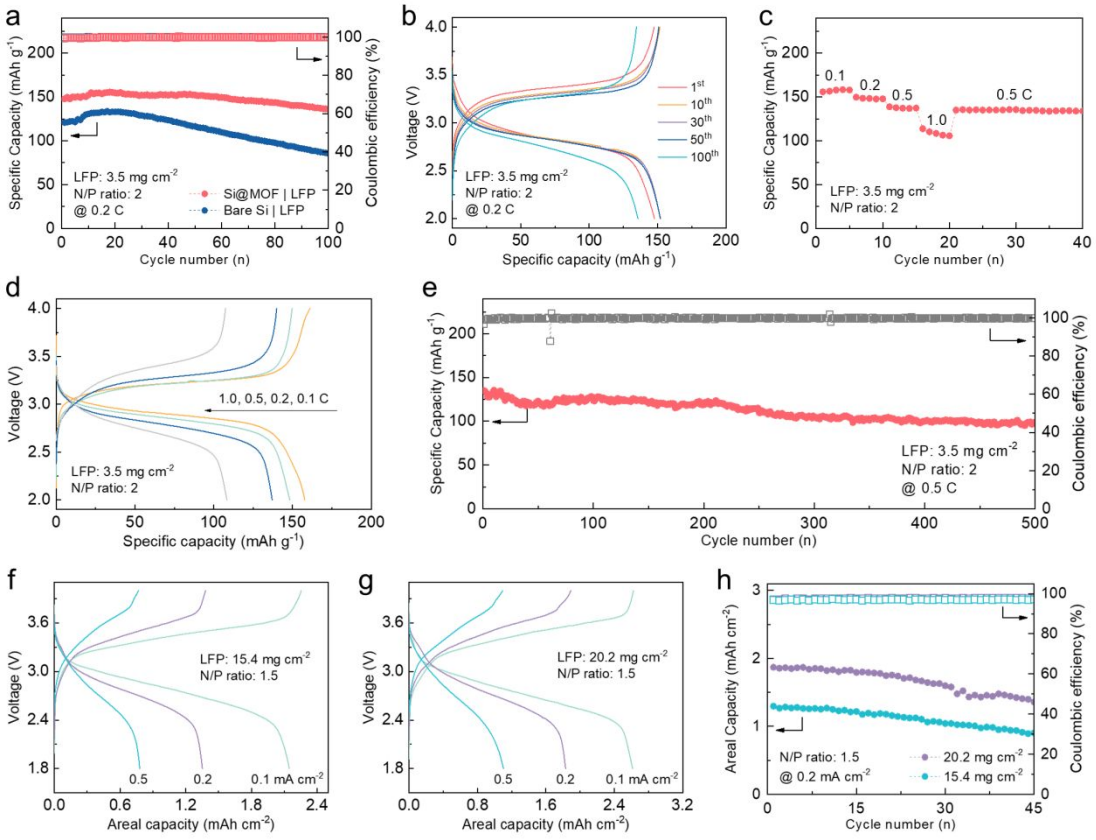

Figure 4. (a) Discharge capacities of full cells using Si@MOF and bare Si electrodes at 0.2 C. (b) Representative voltage profiles of Si@MOF full cell at 0.2 C. (c)

Discharge capacities and (d) voltage profiles of Si@MOF full cell at 0.1, 0.2, 0.5, and 1.0 C. (e) Cycling stability of Si@MOF full cell at 0.5 C for 500 cycles. Voltage profiles of Si@MOF full cells with high LFP loadings of (f) 15.4 and (g) 20.2 mg cm^{-2} at 0.1, 0.2, and 0.5 mA cm^{-2}. (h) Cycling stability of Si@MOF full cells with high LFP loadings at 0.2 mA cm^{-2}. All cells were tested at 60 ℃.

2.4. Electrochemical performance of Si@MOF | PPG | LFP pouch cell

Inspired by the encouraging results from coin cell tests, a pouch cell with the proposed configuration was further fabricated to demonstrate the potential for large-scale implementation. The LFP cathode was 2.5 × 4 cm^2 in size and the loading was 5 mg cm^{-2}. The pouch cell was pressed between two plates fixed by bolts during the cycling test to ensure interfacial contact among all components (Figure S8). Figure 5a shows the discharge capacities at 0.1 and 0.2 C, and reversible capacities of 122 and 111 mAh g^{-1} can be delivered, respectively. Additionally, the cell can be stably cycled for 50 cycles with an average coulombic efficiency of 99.2%. The charge and discharge potentials of the cell remain almost identical to that of coin cells, indicating good reproducibility of the cell performance (Figure 5b). As displayed in Figure 5c, the pouch cell can power the LED light after being folded and even persevere for a while after being cut in the air, which signifies the high safety of our newly developed all-solid-state batteries. Table S1 lists the published works on ASSBs using Li metals anodes and PEO-based SEs for the past few years.[30–32,37–39] It can be concluded that our integrated strategy of combining Si@MOF anode with PPG electrolyte greatly

enhances the long-term cycling stability and high-loading performances of PEO-based ASSBs.

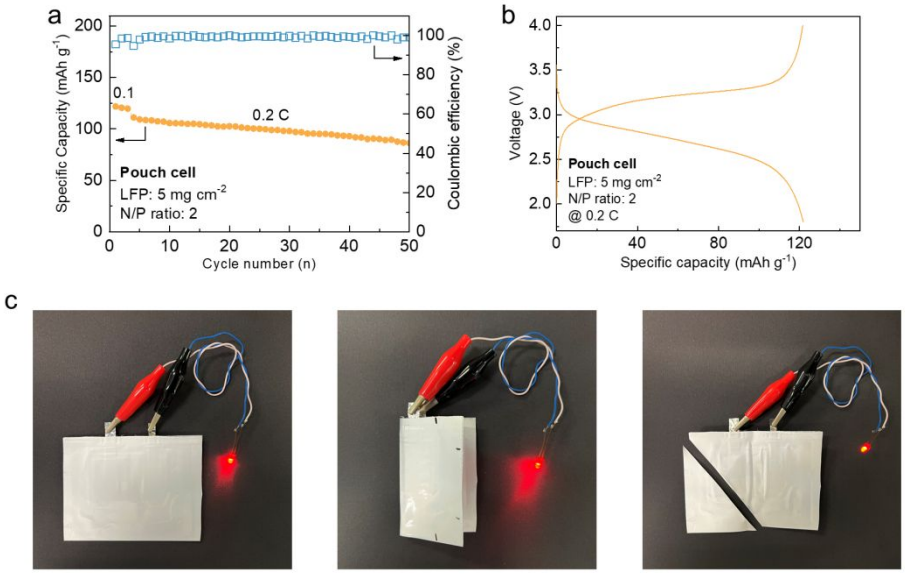

Figure 5. (a) Discharge capacities of Si@MOF | PPG | LFP pouch cell at 0.1 and 0.2 C. (b) Voltage profiles at 0.2 C. (c) Digital photos of the pouch cell powering the LED light after being folded and cut in air.

3. Conclusion

In summary, a long-cycling, high-capacity ASSB using Si@MOF anode paired with PPG solid electrolyte is successfully developed. The MOF-derived carbon host efficiently restrains the repeated deformation of Si nanoparticles, and thus drastically improves the interfacial stability toward the PPG solid electrolyte, which endows the Si@MOF anode with excellent reversibility and high lithiation/delithiation capacity of 3 mAh cm^{-2}. As a result, the full cell using an LFP cathode is able to deliver a high capacity of 148 mAh g^{-1} at the current density of 0.2 C and 60 ℃, and maintains 73.1% of its original capacity after 500 cycles at 0.5 C. More remarkably, the full cells with high LFP loadings achieve high areal capacities of more than 2 mAh cm^{-2}

and show good cycling stability, which surpass most of the reported ASSBs using PEO-based CPEs. In addition, the pouch cell with the proposed configuration represents good electrochemical performance and high safety even under abusive conditions. This work significantly contributes to the development of safe, high-capacity, and long-cycling ASSBs.

4. Experimental Section

4.1. Preparation of Si@MOF

The Si@ZIF-67 was prepared by a hydrothermal method.[34] Typically, 375 mg polyvinylpyrrolidone (PVP) was dissolved in 22.5 mL ethanol, and then 150 mg Si (Average particle size = 100 nm, Sigma Aldrich Inc.) nanoparticles were dispersed in the solution by stirring and ultrasonication treatment. Afterward, the mixture was stirred at room temperature overnight and the Si@PVP was collected by centrifugation. Then, the Si@PVP was re-dispersed thoroughly in the solution of 1.47 g $Co(NO_3)_2 \cdot 6H_2O$ dissolved in 160 mL methanol, followed by the quick adding of 1.67 g 2-methylimidazole to obtain a feed solution. The solution was then heated at 120 ℃ for 4 h in an autoclave and the Si@ZIF-67 was collected by centrifugation and washed with methanol and ethanol several times. Finally, the precursor was calcinated in the Ar gas flow at 800 ℃ for 2 h to get the final Si@MOF product.

4.2. Preparation of PPG solid electrolyte

The PPG was prepared following a method reported by our group previously.[7] The

PVDF fiber network was fabricated by electrospinning. To prepare the PEO solution, 400 mg PEO (M_w = 600,000) and 200 mg lithium bis(trifluoromethanesulfonyl)imide (LiTFSI) were dissolved in 10 mL acetonitrile, and then 80 mg LLZTO nanoparticles (200-400 nm, MTI Co.) were homogeneously dispersed in the solution by ultrasonication, and the mixture was vigorously stirred at 60 ℃ overnight. Afterward, the PEO/LiTFSI/garnet solution was infused into the PVDF network placed on either a polytetrafluorethylene (PTFE) plate (for free-standing PPG) or an LFP cathode, and evaporated at room temperature and then under vacuum at 60 ℃ for 48 h to completely remove the solvent.

4.3. Electrochemical measurements

To prepare the Si@MOF or bare Si anode, the active material, super P, and polyacrylic acid (PAA) binder were mixed in the ethanol with a mass ratio of 7.5:0.5:2 or 6:2:2, and then cast on a copper foil and dried at 60 ℃ under vacuum overnight. The Si loading was 0.6-0.7 mg cm^{-2}. To characterize the Li-Si half cells, CR2032 coin cells were assembled using Li metal, PPG separators, and Si anodes in an Ar-glove box with the H_2O and O_2 less than 0.1 ppm. The cycling tests of the Li-Si half cells were conducted within the voltage window of 0.01-1.5 V (vs. Li/Li^+) on Neware CT-4008W testing equipment. The EIS tests were performed on an electrochemical workstation (Biologic, SP 200) with oscillation frequencies from 7 MHz to 1 Hz.

For the assembly of Si-Si symmetric cells, Si electrodes with a high loading of 4.6

mg cm^{-2} were fabricated to ensure sufficient Li^+ reserve. One Si electrode was lithiated using Li metal and 1 M $LiPF_6$ in ethylene carbonate (EC)/ diethyl carbonate (DEC)(1:1, v/v) and discharged to 0.01 V (vs. Li/Li^+), which was then retrieved from the cell and vacuum dried at 60 ℃ overnight. Afterward, the pre-lithiated Si electrode was paired with another pristine Si electrode separated by PPG in the glove box, and the symmetric cell was allowed to equilibrate to an open circuit voltage (OCV) of 0 V before the following cycling tests.

To prepare the LFP cathode, the $LiFePO_4$ (0.5-3.5 μm, MTI Co.), super P, PEO, and LiTFSI were mixed in the acetonitrile with a mass ratio of 8:1:0.75:0.25, and then cast on a carbon-coated aluminum foil and dried at 60 ℃ under vacuum overnight. To ensure the intimate interfacial contact between cathode and PPG, the PVDF network was directly pressed on the LFP cathode followed by the infusion of PEO solution to obtain an integrated PPG-LFP structure.[7] For the full cell assembly, the Si anodes were firstly lithiated using Li metal and 1 M LiPF6 in EC/DEC (1:1, v/v) with designated capacities and then retrieved from the cell and vacuum dried at 60 ℃ overnight. Afterward, the pre-lithiated Si anodes were paired with PPG-LFP in the glove box. The cycling tests of the Si | PPG | LFP full cells were conducted within the voltage window of 2.0-4.0 V. For the pouch cell assembly, The LFP-PPG integrated cathode was 2.5 × 4 cm^2 in size and the LFP loading was 5 mg cm^{-2}. The Si@MOF anode was 2 × 3.5 cm^2 in size to ensure its total coverage by the cathode, which was lithiated with designated capacity. The pouch cell was pressed between two plates fixed by bolts during the cycling test to ensure interfacial contact among all

components (Figure S8).

Supporting Information

Additional experimental details; SEM and TGA of Si@MOF; XRD and ionic conductivity of PPG; voltage profiles of Li | PPG | Li and bare Si symmetric cell; comparison of recent works on PEO-based ASSBs.

Conflicts of interest

The authors declare no competing financial interest.

Acknowledgments

The work described in this paper was fully supported by a grant from the Research Grants Council of the Hong Kong Special Administrative Region, China (Project No. R6005-20).

References

(1) Liu, J.; Bao, Z.; Cui, Y.; Dufek, E. J.; Goodenough, J. B.; Khalifah, P.; Li, Q.; Liaw, B. Y.; Liu, P.; Manthiram, A.; Meng, Y. S.; Subramanian, V. R.; Toney, M. F.; Viswanathan, V. V.; Whittingham, M. S.; Xiao, J.; Xu, W.; Yang, J.; Yang, X. Q.; Zhang, J. G. Pathways for Practical High-Energy Long-Cycling Lithium Metal Batteries. *Nat. Energy* **2019**, *4* (3), 180–186. https://doi.org/10.1038/s41560-019-0338-x.

(2) Liu, T.; Yuan, Y.; Tao, X.; Lin, Z.; Lu, J. Bipolar Electrodes for Next-Generation Rechargeable Batteries. *Adv. Sci.* **2020**, *7* (17), 1–13. https://doi.org/10.1002/advs.202001207.

(3) Yu, Z.; Wang, H.; Kong, X.; Huang, W.; Tsao, Y.; Mackanic, D. G.; Wang, K.; Wang, X.; Huang, W.; Choudhury, S.; Zheng, Y.; Amanchukwu, C. V.; Hung, S. T.; Ma, Y.; Lomeli, E. G.; Qin, J.; Cui, Y.; Bao, Z. Molecular Design for Electrolyte Solvents Enabling Energy-Dense and Long-Cycling Lithium Metal Batteries. *Nat. Energy* **2020**, *5* (7), 526–533. https://doi.org/10.1038/s41560-020-0634-5.

(4) Zheng, X.; Huang, L.; Luo, W.; Wang, H.; Dai, Y.; Liu, X.; Wang, Z.; Zheng, H.; Huang, Y. Tailoring Electrolyte Solvation Chemistry toward an Inorganic-Rich Solid-Electrolyte Interphase at a Li Metal Anode. *ACS Energy Lett.* **2021**, *6* (6), 2054–2063. https://doi.org/10.1021/acsenergylett.1c00647.

(5) Shen, X.; Zhang, X.-Q.; Ding, F.; Huang, J.-Q.; Xu, R.; Chen, X.; Yan, C.; Su, F.-Y.; Chen, C.-M.; Liu, X.; Zhang, Q. Advanced Electrode Materials in Lithium Batteries: Retrospect and Prospect. *Energy Mater. Adv.* **2021**, *2021*, 1–15. https://doi.org/10.34133/2021/1205324.

(6) Xu, L.; Li, J.; Deng, W.; Shuai, H.; Li, S.; Xu, Z.; Li, J.; Hou, H.; Peng, H.; Zou, G.; Ji, X. Garnet Solid Electrolyte for Advanced All-Solid-State Li Batteries. *Adv. Energy Mater.* **2021**, *11* (2), 1–24. https://doi.org/10.1002/aenm.202000648.

(7) Lin, Y.; Wu, M.; Sun, J.; Zhang, L.; Jian, Q.; Zhao, T. A High-Capacity, Long-

Cycling All-Solid-State Lithium Battery Enabled by Integrated Cathode/Ultrathin Solid Electrolyte. *Adv. Energy Mater.* **2021**, *11* (35), 1–9. https://doi.org/10.1002/aenm.202101612.

(8) Li, Q.; Yi, T.; Wang, X.; Pan, H.; Quan, B.; Liang, T.; Guo, X.; Yu, X.; Wang, H.; Huang, X.; Chen, L.; Li, H. In-Situ Visualization of Lithium Plating in All-Solid-State Lithium-Metal Battery. *Nano Energy* **2019**, *63* (June), 103895. https://doi.org/10.1016/j.nanoen.2019.103895.

(9) Kasemchainan, J.; Zekoll, S.; Spencer Jolly, D.; Ning, Z.; Hartley, G. O.; Marrow, J.; Bruce, P. G. Critical Stripping Current Leads to Dendrite Formation on Plating in Lithium Anode Solid Electrolyte Cells. *Nat. Mater.* **2019**, *18* (10), 1105–1111. https://doi.org/10.1038/s41563-019-0438-9.

(10) Dunlap, N. A.; Kim, J.; Guthery, H.; Jiang, C.-S.; Morrissey, I.; Stoldt, C. R.; Oh, K. H.; Al-Jassim, M.; Lee, S.-H. Towards the Commercialization of the All-Solid-State Li-Ion Battery: Local Bonding Structure and the Reversibility of Sheet-Style Si-PAN Anodes. *J. Electrochem. Soc.* **2020**, *167* (6), 060522. https://doi.org/10.1149/1945-7111/ab84fc.

(11) Zhang, L.; Zhao, C.; Jian, Q.; Wu, M.; Zhao, T. A High-Performance Lithiated Silicon–Sulfur Battery with Pomegranate-Structured Electrodes. *J. Power Sources* **2021**, *506* (April), 230174. https://doi.org/10.1016/j.jpowsour.2021.230174.

(12) Zhang, X.; Wang, D.; Qiu, X.; Ma, Y.; Kong, D.; Müllen, K.; Li, X.; Zhi, L. Stable High-Capacity and High-Rate Silicon-Based Lithium Battery Anodes

upon Two-Dimensional Covalent Encapsulation. *Nat. Commun.* **2020**, *11* (1), 1–9. https://doi.org/10.1038/s41467-020-17686-4.

(13) Xu, W.; Tang, C.; Huang, N.; Du, A.; Wu, M.; Zhang, J.; Zhang, H. Adina Rubella-Like Microsized SiO@N-Doped Carbon Grafted with N-Doped Carbon Nanotubes as Anodes for High-Performance Lithium Storage. *Small Sci.* **2022**, *2* (4), 2100105. https://doi.org/10.1002/smsc.202100105.

(14) Chen, J.; Fan, X.; Li, Q.; Yang, H.; Khoshi, M. R.; Xu, Y.; Hwang, S.; Chen, L.; Ji, X.; Yang, C.; He, H.; Wang, C.; Garfunkel, E.; Su, D.; Borodin, O.; Wang, C. Electrolyte Design for LiF-Rich Solid–Electrolyte Interfaces to Enable High-Performance Microsized Alloy Anodes for Batteries. *Nat. Energy* **2020**, *5* (5), 386–397. https://doi.org/10.1038/s41560-020-0601-1.

(15) Zhang, L.; Zhao, C.; Lin, Y.; Wu, M.; Zhao, T. A High-Performance Lithiated Silicon-Sulfur Battery Enabled by Fluorinated Ether Electrolytes. *J. Mater. Chem. A* **2021**, *9* (45), 25426–25434. https://doi.org/10.1039/d1ta05734k.

(16) Cervera, R. B.; Suzuki, N.; Ohnishi, T.; Osada, M.; Mitsuishi, K.; Kambara, T.; Takada, K. High Performance Silicon-Based Anodes in Solid-State Lithium Batteries. *Energy Environ. Sci.* **2014**, *7* (2), 662–666. https://doi.org/10.1039/c3ee43306d.

(17) Miyazaki, R.; Ohta, N.; Ohnishi, T.; Sakaguchi, I.; Takada, K. An Amorphous Si Film Anode for All-Solid-State Lithium Batteries. *J. Power Sources* **2014**, *272*, 541–545. https://doi.org/10.1016/j.jpowsour.2014.08.109.

(18) Chen, C.; Li, Q.; Li, Y.; Cui, Z.; Guo, X.; Li, H. Sustainable Interfaces between

Si Anodes and Garnet Electrolytes for Room-Temperature Solid-State Batteries. *ACS Appl. Mater. Interfaces* **2018**, *10* (2), 2185–2190. https://doi.org/10.1021/acsami.7b16385.

(19) Ferraresi, G.; El Kazzi, M.; Czornomaz, L.; Tsai, C. L.; Uhlenbruck, S.; Villevieille, C. Electrochemical Performance of All-Solid-State Li-Ion Batteries Based on Garnet Electrolyte Using Silicon as a Model Electrode. *ACS Energy Lett.* **2018**, *3* (4), 1006–1012. https://doi.org/10.1021/acsenergylett.8b00264.

(20) Ping, W.; Yang, C.; Bao, Y.; Wang, C.; Xie, H.; Hitz, E.; Cheng, J.; Li, T.; Hu, L. A Silicon Anode for Garnet-Based All-Solid-State Batteries: Interfaces and Nanomechanics. *Energy Storage Mater.* **2019**, *21* (December 2018), 246–252. https://doi.org/10.1016/j.ensm.2019.06.024.

(21) Sakabe, J.; Ohta, N.; Ohnishi, T.; Mitsuishi, K.; Takada, K. Porous Amorphous Silicon Film Anodes for High-Capacity and Stable All-Solid-State Lithium Batteries. *Commun. Chem.* **2018**, *1* (1), 1–9. https://doi.org/10.1038/s42004-018-0026-y.

(22) Cangaz, S.; Hippauf, F.; Reuter, F. S.; Doerfler, S.; Abendroth, T.; Althues, H.; Kaskel, S. Enabling High-Energy Solid-State Batteries with Stable Anode Interphase by the Use of Columnar Silicon Anodes. *Adv. Energy Mater.* **2020**, *10* (34). https://doi.org/10.1002/aenm.202001320.

(23) Tan, D. H. S.; Chen, Y. T.; Yang, H.; Bao, W.; Sreenarayanan, B.; Doux, J. M.; Li, W.; Lu, B.; Ham, S. Y.; Sayahpour, B.; Scharf, J.; Wu, E. A.; Deysher, G.;

Han, H. E.; Hah, H. J.; Jeong, H.; Lee, J. B.; Chen, Z.; Meng, Y. S. Carbon-Free High-Loading Silicon Anodes Enabled by Sulfide Solid Electrolytes. *Science (80-.).* **2021**, *373* (6562), 1494–1499. https://doi.org/10.1126/science.abg7217.

(24) Zou, Z.; Li, Y.; Lu, Z.; Wang, D.; Cui, Y.; Guo, B.; Li, Y.; Liang, X.; Feng, J.; Li, H.; Nan, C. W.; Armand, M.; Chen, L.; Xu, K.; Shi, S. Mobile Ions in Composite Solids. *Chem. Rev.* **2020**, *120* (9), 4169–4221. https://doi.org/10.1021/acs.chemrev.9b00760.

(25) Yang, X.; Adair, K. R.; Gao, X.; Sun, X. Recent Advances and Perspectives on Thin Electrolytes for High-Energy-Density Solid-State Lithium Batteries. *Energy Environ. Sci.* **2021**, *14* (2), 643–671. https://doi.org/10.1039/d0ee02714f.

(26) Kong, L.; Tang, C.; Peng, H.; Huang, J.; Zhang, Q. Advanced Energy Materials for Flexible Batteries in Energy Storage: A Review. *SmartMat* **2020**, *1* (1). https://doi.org/10.1002/smm2.1007.

(27) Zhou, D.; Shanmukaraj, D.; Tkacheva, A.; Armand, M.; Wang, G. Polymer Electrolytes for Lithium-Based Batteries: Advances and Prospects. *Chem* **2019**, *5* (9), 2326–2352. https://doi.org/10.1016/j.chempr.2019.05.009.

(28) Xue, Z.; He, D.; Xie, X. Poly(Ethylene Oxide)-Based Electrolytes for Lithium-Ion Batteries. *J. Mater. Chem. A* **2015**, *3* (38), 19218–19253. https://doi.org/10.1039/c5ta03471j.

(29) Pan, H.; Cheng, Z.; He, P.; Zhou, H. A Review of Solid-State Lithium-Sulfur

Battery: Ion Transport and Polysulfide Chemistry. *Energy and Fuels* **2020**, *34* (10), 11942–11961. https://doi.org/10.1021/acs.energyfuels.0c02647.

(30) Ban, X.; Zhang, W.; Chen, N.; Sun, C. A High-Performance and Durable Poly(Ethylene Oxide)-Based Composite Solid Electrolyte for All Solid-State Lithium Battery. *J. Phys. Chem. C* **2018**, *122* (18), 9852–9858. https://doi.org/10.1021/acs.jpcc.8b02556.

(31) Wan, Z.; Lei, D.; Yang, W.; Liu, C.; Shi, K.; Hao, X.; Shen, L.; Lv, W.; Li, B.; Yang, Q. H.; Kang, F.; He, Y. B. Low Resistance–Integrated All-Solid-State Battery Achieved by Li7La3Zr2O12 Nanowire Upgrading Polyethylene Oxide (PEO) Composite Electrolyte and PEO Cathode Binder. *Adv. Funct. Mater.* **2019**, *29* (1), 1–10. https://doi.org/10.1002/adfm.201805301.

(32) Chen, H.; Adekoya, D.; Hencz, L.; Ma, J.; Chen, S.; Yan, C.; Zhao, H.; Cui, G.; Zhang, S. Stable Seamless Interfaces and Rapid Ionic Conductivity of Ca–CeO2/LiTFSI/PEO Composite Electrolyte for High-Rate and High-Voltage All-Solid-State Battery. *Adv. Energy Mater.* **2020**, *10* (21), 1–13. https://doi.org/10.1002/aenm.202000049.

(33) Wang, C.; Wang, T.; Wang, L.; Hu, Z.; Cui, Z.; Li, J.; Dong, S.; Zhou, X.; Cui, G. Differentiated Lithium Salt Design for Multilayered PEO Electrolyte Enables a High-Voltage Solid-State Lithium Metal Battery. *Adv. Sci.* **2019**, *6* (22). https://doi.org/10.1002/advs.201901036.

(34) Gao, R.; Tang, J.; Yu, X.; Tang, S.; Ozawa, K.; Sasaki, T.; Qin, L. C. In Situ Synthesis of MOF-Derived Carbon Shells for Silicon Anode with Improved

Lithium-Ion Storage. *Nano Energy* **2020**, *70* (November 2019), 1–2. https://doi.org/10.1016/j.nanoen.2019.104444.

(35) Tang, J.; Salunkhe, R. R.; Liu, J.; Torad, N. L.; Imura, M.; Furukawa, S.; Yamauchi, Y. Thermal Conversion of Core-Shell Metal-Organic Frameworks: A New Method for Selectively Functionalized Nanoporous Hybrid Carbon. *J. Am. Chem. Soc.* **2015**, *137* (4), 1572–1580. https://doi.org/10.1021/ja511539a.

(36) Li, S.; Zhang, S. Q.; Shen, L.; Liu, Q.; Ma, J. Bin; Lv, W.; He, Y. B.; Yang, Q. H. Progress and Perspective of Ceramic/Polymer Composite Solid Electrolytes for Lithium Batteries. *Adv. Sci.* **2020**, *7* (5). https://doi.org/10.1002/advs.201903088.

(37) Huo, H.; Chen, Y.; Luo, J.; Yang, X.; Guo, X.; Sun, X. Rational Design of Hierarchical "Ceramic-in-Polymer" and "Polymer-in-Ceramic" Electrolytes for Dendrite-Free Solid-State Batteries. *Adv. Energy Mater.* **2019**, *9* (17), 1–8. https://doi.org/10.1002/aenm.201804004.

(38) Bi, Z.; Mu, S.; Zhao, N.; Sun, W.; Huang, W.; Guo, X. Cathode Supported Solid Lithium Batteries Enabling High Energy Density and Stable Cyclability. *Energy Storage Mater.* **2021**, *35* (November 2020), 512–519. https://doi.org/10.1016/j.ensm.2020.11.038.

(39) Liu, Y.; Hu, R.; Zhang, D.; Liu, J.; Liu, F.; Cui, J.; Lin, Z.; Wu, J.; Zhu, M. Constructing Li-Rich Artificial SEI Layer in Alloy–Polymer Composite Electrolyte to Achieve High Ionic Conductivity for All-Solid-State Lithium Metal Batteries. *Adv. Mater.* **2021**, *33* (11), 29–31.

https://doi.org/10.1002/adma.202004711.

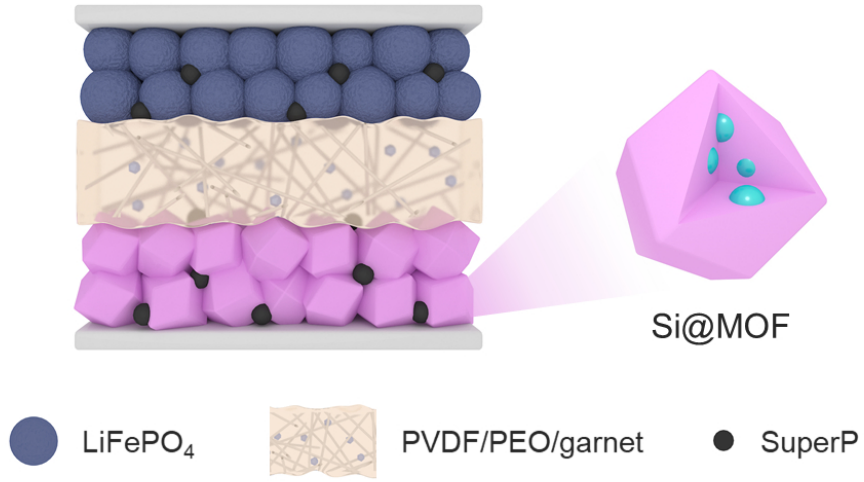

Table of content

82x44mm (300 x 300 DPI)

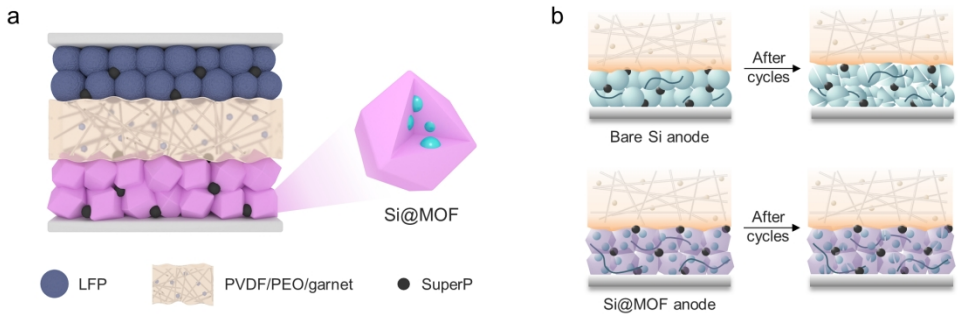

Figure 1. Schematic illustration of (a) the ASSB comprised of LFP | PVDF/PEO/garnet (PPG) | Si@MOF and (b) interfacial evolution between PPG and bare Si or Si@MOF anode.

177x60mm (300 x 300 DPI)

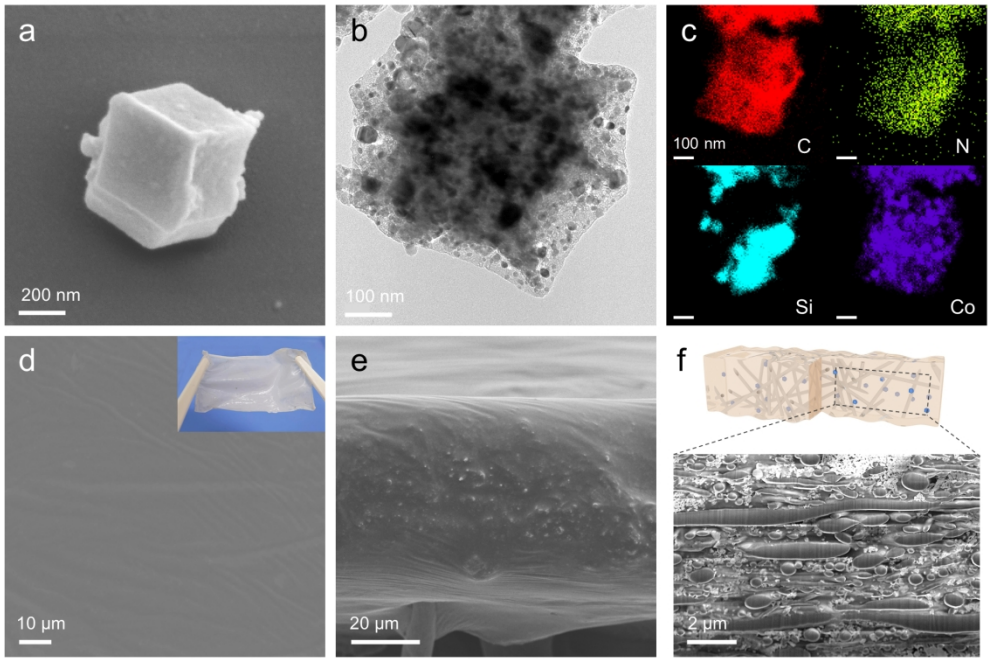

Figure 2. (a) SEM and (b) TEM image of Si@MOF structure and corresponding (c) EDS element mapping results of C, N, Si, and Co. SEM images of PPG from the (d) top and (e) cross-sectional views. Inset in (d) is the digital photo of PPG. (f) The inner structure of PPG after FIB cutting.

177x119mm (300 x 300 DPI)

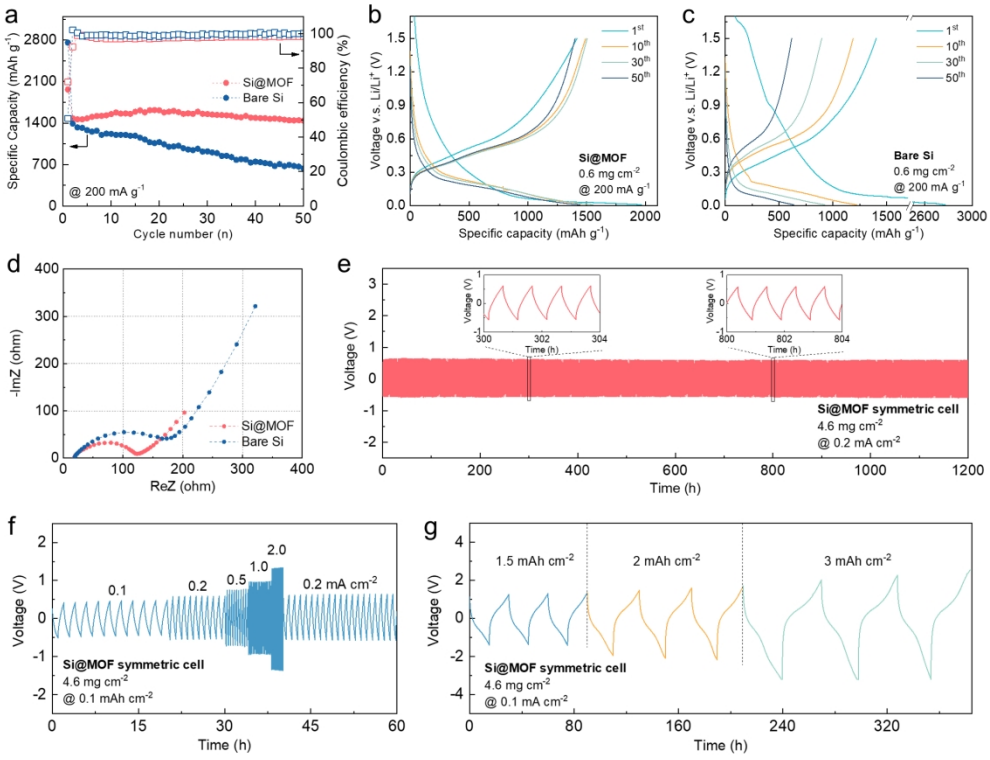

Figure 3. (a) Lithiation capacities of Si@MOF and bare Si electrode at 200 mA g^{-1}. Representative voltage profiles of (b) Si@MOF and (c) bare Si electrodes. (d) Nyquist plots of two electrodes after activation cycles. Voltage profiles of Si@MOF symmetric cell cycling at (e) 0.2 mA cm^{-2} for 1200 h, (f) varying current densities, and (g) 1.5, 2, and 3 mAh cm^{-2} for 3 cycles each at 0.1 mA cm^{-2}. The cells were tested at 60 ℃.

177x134mm (300 x 300 DPI)

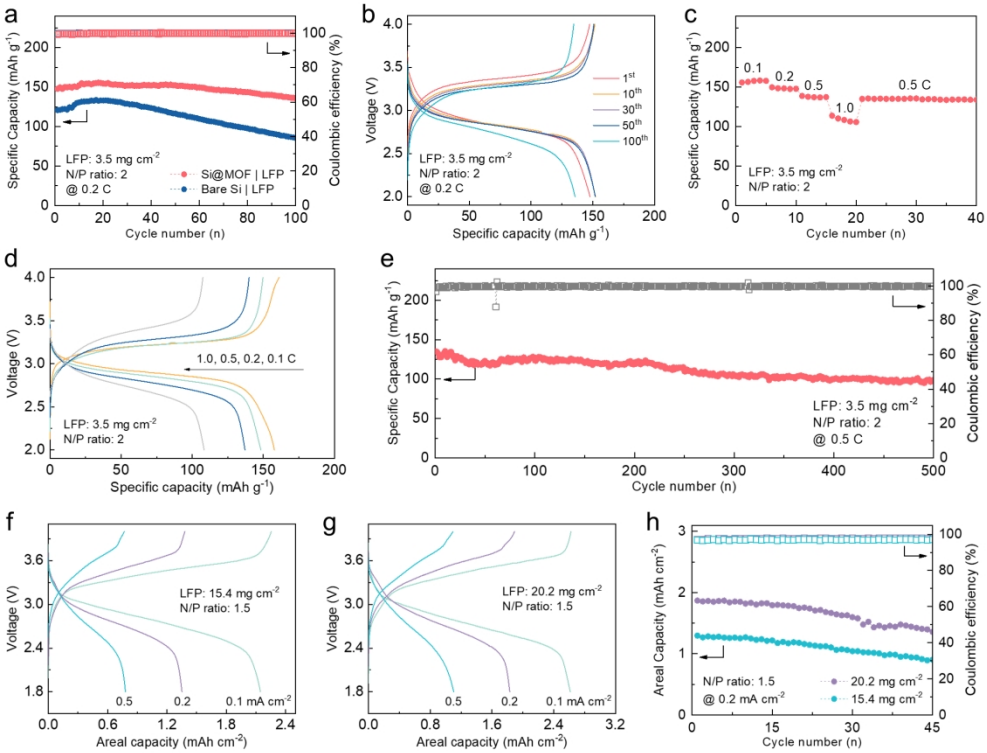

Figure 4. (a) Discharge capacities of full cells using Si@MOF and bare Si electrodes at 0.2 C. (b) Representative voltage profiles of Si@MOF full cell at 0.2 C. (c) Discharge capacities and (d) voltage profiles of Si@MOF full cell at 0.1, 0.2, 0.5, and 1.0 C. (e) Cycling stability of Si@MOF full cell at 0.5 C for 500 cycles. Voltage profiles of Si@MOF full cells with high LFP loadings of (f) 15.4 and (g) 20.2 mg cm^{-2} at 0.1, 0.2, and 0.5 mA cm^{-2}. (h) Cycling stability of Si@MOF full cells with high LFP loadings at 0.2 mA cm^{-2}. All cells were tested at 60 ℃.

177x134mm (300 x 300 DPI)

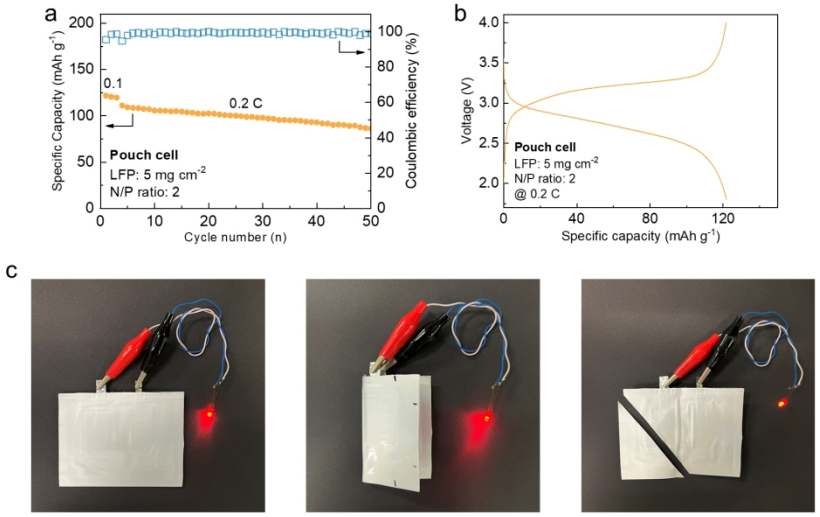

Figure 5. (a) Discharge capacities of Si@MOF | PPG | LFP pouch cell at 0.1 and 0.2 C. (b) Voltage profiles at 0.2 C. (c) Digital photos of the pouch cell powering the LED light after being folded and cut in air.

177x92mm (300 x 300 DPI)